



An Innovative Mechanism of Directional Rock Cracking Mechanics and Mine Pressure Control Method for Energy-Gathering Blasting

Xiaoding Xu¹ · Yuejin Zhou¹ · Jun Yang² · Yubing Gao² · Chun Zhu³ · Yajun Wang² · Qiang Fu²

Received: 12 December 2023 / Accepted: 25 May 2024

© The Author(s), under exclusive licence to Springer-Verlag GmbH Austria, part of Springer Nature 2024, corrected publication 2024

Abstract

The extraction of thick coal seams at high intensity inevitably leads to more severe strata pressure, especially when influenced by adjacent goaf areas. The combination of multiple strata pressures results in significant deformation of the surrounding rock along the goaf roadway. In order to the problem of large deformation of the surrounding rock of the gob-side roadway, this study proposes a novel method for protecting gob-side roadway using energy-gathering blasting (EGB) to cut roof and relieve pressure, which combines parallel pull-rods fracture theory with the Weibull strength of rock microelements to establish a new energy-gathering blasting model. The optimal spacing of blast holes is determined and the correlation between damage degree and energy-absorbing coefficient as well as explosive center distance is analyzed. Numerical simulation methods are employed for validation, and the results demonstrate that the EGB technique effectively blocks the transmission of stress in non-energy-absorbing directions, further enhancing energy accumulation in the energy-gathering direction. This leads to slower attenuation of effective stress and particle vibration velocity in the energy-gathering direction, promoting the directional expansion of energy-gathering fractures and revealing the mechanical mechanism of energy-gathering fracture directional expansion. Based on this technology, a method for relieving overburden pressure in the surrounding rock is proposed. Through EGB technique cutting the long cantilever structure of thick and hard rock layers is snapped, force them to collapse and expand, thereby supporting the overlying structure and reducing stress concentration in the roadway's surrounding rock. This method reveals the mechanism of pressure unloading in the mining area after roof cutting. Furthermore, based on theoretical analysis, the parameters for roof-cutting pressure unloading are designed, and engineering practice confirms the successful reduction of stress on both sides of the roadway ahead of the working face, optimizing the stress environment of the roadway and achieving the goal of protecting the tests have validated the effectiveness of the method, significantly reducing stress and deformation in the surrounding rock of the roadway. The research findings provide a scientific basis for controlling roadway deformation under similar conditions.

Highlights

- A new EGB method is proposed based on characteristics of rock.
- A novel damage model for EGB has been constructed by combining the rock micro element strength with the tension rod fracture theory.
- The application of EGB method in coal mining can effectively reduce mine pressure and protect roadway.

Keywords Roof cutting and pressure relief · Energy-gathering blasting · Parallel tie rod · Directional fracturing · Energy dissipation · Weibull function

✉ Xiaoding Xu
ding_xu@cumt.edu.cn

✉ Yubing Gao
ybinggao@yahoo.com

² State Key Laboratory for Geomechanics and Deep Underground Engineering Beijing, China University of Mining and Technology, Beijing 100083, China

³ School of Earth Sciences and Engineering, Hohai University, Nanjing 210098, China

¹ State Key Laboratory of Intelligent Construction and Healthy Operation and Maintenance of Deep Underground Engineering, University of Mining and Technology, Xuzhou 221008, China

1 Introduction

The EGB technology is a novel technique for directional rock fracturing, which exploits the mechanical characteristic that the tensile strength of rocks is significantly lower than their compressive strength. By employing a special energy-concentrating device to accumulate and release energy in a specific direction, this technique induces directional cracking in rocks, preventing the uncontrolled propagation of fractures. It finds extensive applications in areas such as roof-cut unloading protective roadways, erosion prevention, and pillar-free mining. However, the current engineering application of this technology relies on field experience and trial results to design operational parameters. Often, each project requires on-site experiments to determine the charge quantity and borehole spacing, resulting in substantial wastage of manpower, financial resources, and time. Moreover, due to the unclear mechanics behind directional fracturing, improper selection of operational parameters may lead to significant engineering safety accidents. Therefore, conducting research on the energy-concentrating directional fracturing mechanism and damage degree is not only conducive to parameter design but also holds great significance for ensuring engineering safety.

Due to the immediacy, intricacy, and indistinctness of the blasting process, there exist numerous research theories in this domain, and a plethora of conjectures and calculation formulas for rock blasting mechanisms have been postulated (Yang et al. 2020; Xu et al. 2020; Yang et al. 2014; Hu et al. 2012). These suppositions, to a certain extent, divulge certain characteristics of failure and laws of rock masses. Independently, G. Harris considered the impact of stress waves and amalgamated it with the theory of continuous media to establish a two-dimensional paradigm of rock failure damage under uniform circumstances, scrutinizing the pattern of crack propagation (Harris and Hengst 1977). R. F. Favreau dissected the law of damage in rocks under the coupling effect of stress waves and explosive gas and devised a three-dimensional mechanical archetype for explosive crack propagation. Founded on the analysis of blasting crack propagation (Favreau 1969). Taylor et al. formulated a blasting damage model connected to crack density, namely the TCK model, employing crack density as the criterion (Taylor et al. 1986). Thorne et al. analyzed the enlargement of rock volume instigated by the expansion of rock cracks subsequent to blasting, and subsequently defined the rule for judging damage to rocks, erecting a rock blasting damage model dependent on the condition of extensive crack propagation at the micro level (Thorne et al. 1990). Xu et al. scrutinized the influence of time on crack density based on the Thorne model and devised a blasting damage model with temporal parameters (Xu et al. 2019). Kuzman established a rock damage criterion associated with crack density and applied percolation theory to analyze the distribution of

rock damage fragmentation after blasting (Kuzmaul 1987). Grady and Kipp contrived a GK model to ascertain rock damage through crack propagation, and derived the correlation between rock strain rate and the size of fractured rock founded on energy theory analysis (Grady and Kipp 1987). In China, a multitude of scholars have also conducted comprehensive research on blasting damage (Chu et al. 2014; Kang et al. 2019; Jiang et al. 2020; Xu 2019; He et al. 2018; Gao et al., 2019). Zou employed energy theory to construct a step-by-step blasting damage model connected to rock surface failure energy, and examined the size of fractured rock mass caused by blasting (Zou 1985). Yang et al. constructed a two-stage damage model for blasting, positing that rock damage is triggered by the collective effects of stress waves and explosive gas. Yang et al. analyzed the dissipation law of sound waves during the process of rock blasting damage and introduced fractal theory into the realm of blasting damage investigation (Yang 2000; Yang and Jin 2018). Shan et al. conducted similarity simulation experiments to scrutinize the alterations in ultrasonic velocity before and after blasting and assessed the extent of damage to the model based on this (Shan et al. 2014).

In the aforementioned research regarding conventional blasting, the zone of destruction is categorized into fracture, crack, and vibration zones. Nevertheless, the mechanisms of damage caused by EGB and non-EGB differ, with the fracture zone being less prominent, predominantly resulting in the formation of tensile cracks within the rock. Consequently, traditional blasting theories are inadequate for analyzing the fracture mechanisms and degree of damage resulting from EGB. Therefore, this article is grounded upon the energy dissipation theory of parallel rod fracture theory, combined with the Weibull function distribution of rock micro-element strength, to establish a mechanical model for rod damage in EGB. Subsequently, the mechanisms of cracking in EGB are analyzed, thereby supplementing the fundamental research on directional cracking theory in EGB. This holds substantial practical significance for parameter design and safety assurance in subsequent stages.

2 Analysis of the Directional Cracking Mechanism of EGB

2.1 Principle of EGB Technology

The EGB technology effectively exploits the mechanical properties of rocks, whereby their compressive strength far surpasses their tensile strength. Additionally, a shaped energy device is incorporated into the borehole, as depicted in Fig. 1, to direct the release of energy in a specific direction. The energy-capturing tube can alter the direction of shock waves and explosive gases resulting from the blasting.

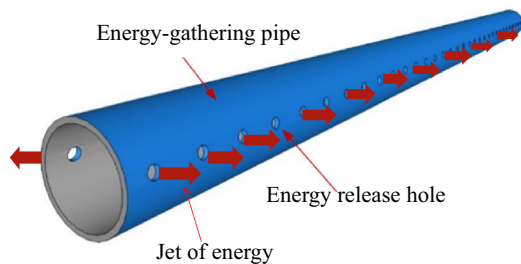


Fig. 1 Schematic diagram of blasting energy-gathering pipe

Under the influence of the energy-capturing tube, the blasting energy forms a jet along the release direction of the borehole, intensifying the force exerted on the borehole wall by the blasting. Conversely, in the non-energy-gathering direction, the energy-capturing tube can mitigate the impact of blasting products on the borehole wall, thereby diminishing the force exerted on the surrounding rock mass in the non-energy-gathering direction. Hence, directional fracturing can be achieved while preserving the integrity of the surrounding rock in the non-energy-gathering direction (Xu et al. 2018; Xu et al. 2023; Shi et al. 2020).

The comparative illustration depicting the energy release and crack propagation between non-EGB and EGB are displayed in Fig. 2.

The efficacy of EGB technology can be ascertained through on-site experiments conducted in the field of blasting engineering. In this particular experiment, the roof rock comprises sandstone, boasting a uniaxial compressive strength ranging from 50 to 80 MPa. Furthermore, the drilling depth measures is 7 m, the charging length is 5.5 m, while the sealing length encompasses is 1.5 m. The drilling diameter amounts to 50 mm, and the drilling spacing is set at 500 mm. The drill holes are arranged sequentially in a row. Secondary emulsion explosives serve as the explosive material, and non-electric millisecond detonators are employed to simultaneously ignite the drilled holes. Post-blasting, the surface cracks in the blasted hole sever the roof rock along the designated direction of energy accumulation. Simultaneously, drilling and peeping equipment are employed to scrutinize the cracks present within the hole. The resulting blasting effect is visually represented in Fig. 3. Upon examination, it is discernible that cracks manifest in two directions aligned with the designated direction of energy accumulation, while no visible cracks materialize in alternative directions.

In summary, the revolutionary EGB technique possesses the ability to effectively govern the expansion direction of blasting fractures and cleave through formidable, robust roof slabs in the desired orientation. Moreover, this blasting procedure does not compromise the structural integrity of the roadway overhead.

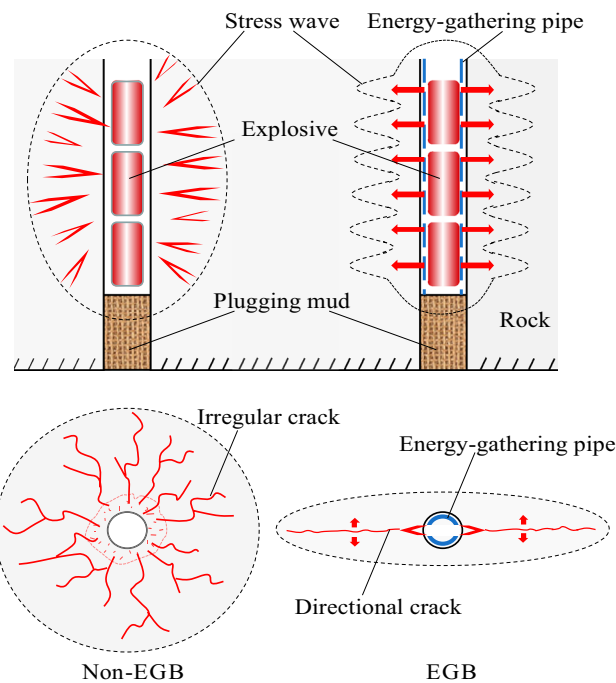


Fig. 2 Comparison of fracture mechanism between non-EGB and EGB

2.2 A Mechanical Model of EGB

The rock masses residing between the strategically positioned EGB orifices endure a state of tensile fracture while adhering to a fixed trajectory of crack propagation. By emulating the intricate microcosmic components of the rock matrix between these two openings, a collection of parallel, brittle traction rods is erected, mirroring their behavior. Each and every one of these fracture rods harbors an intact elastic constitution until it attains its ultimate tensile strength. It is at this juncture that the rod undergoes a split, marking the onset of crack propagation, exemplified in Fig. 4.

Assuming that the stiffness of brittle tie rods is k/N , the deformation relationship of the tie rods is

$$f_n = \begin{cases} \frac{k\varepsilon}{N} & 0 \leq \frac{k\varepsilon}{N} \leq \sigma_T \\ 0 & \frac{k\varepsilon}{N} \geq \sigma_T \end{cases} \quad (1)$$

where σ_T is the ultimate tensile strength of the rod; ε is the axial displacement of the rod.

Optimizing the inter-hole distance pertaining to the arrangement of EGB apertures proffers not only the facilitation of stress relief, but also an abatement in the squandering of valuable blasting energy. Consequently, the fine-tuning of this inter-hole spacing assumes paramount importance. Since stress wave attenuation transpires along

Fig. 3 Test blasting effect

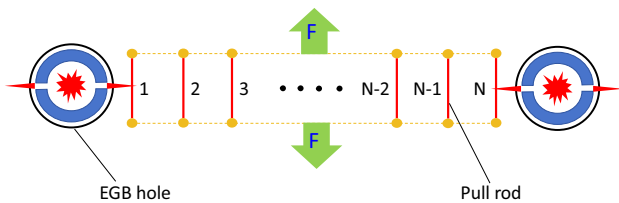
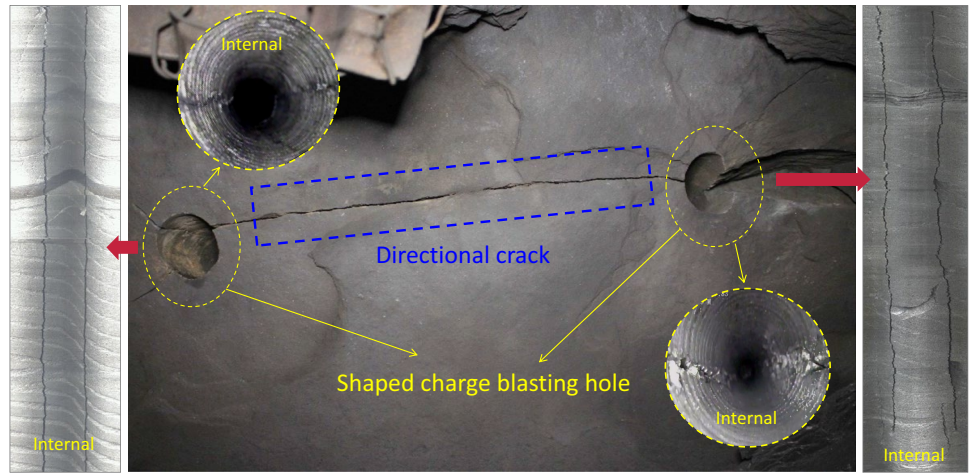


Fig. 4 Mechanical model of parallel pull rod fracture

the distance direction post-blast, the moment the attenuated stress surpasses the threshold of tensile strength, the ensuing tensile fracture commences its expansion. To effectuate the permeation of cracks between holes, it remains imperative to computationally determine the optimal hole-spacing by solving for the condition where the cumulative, superimposed stress surmounts the tensile strength of the central point tension rod.

The radial stress of the hole wall under the combined action of blasting stress wave and explosive gas is:

$$\sigma_0 = \frac{1}{8} \lambda n \rho_0 V_{\max}^2 \left(\frac{d_c}{d_b} \right)^6 = \frac{1}{8} \lambda n \rho_0 V_{\max}^2 \left(\frac{1}{K_d} \right)^6 \quad (2)$$

where σ_0 is the radial stress of the hole, ρ_0 is the density of the explosive, K_d is the uncoupled charge coefficient, λ is the coefficient of energy-gathering; n is the coefficient of increase in explosive gas pressure, d_c is the diameter of the explosive, d_b is the diameter of the blasting hole, V_{\max} is the maximum detonation velocity of the explosive.

The attenuation law of stress peak along the direction of energy-gathering is

$$\sigma_r = \sigma_0 \left(\frac{r}{r_0} \right)^{-\alpha} \quad (3)$$

where σ_r is the peak stress, r is the distance from the center of the explosion; r_0 is the charge radius, and α is the attenuation coefficient.

$$\alpha = 2 - \frac{\mu}{1 - \mu} \quad (4)$$

where μ is the Poisson's ratio of the rock.

The stress superposition value at any position in the direction of energy-gathering under the action of dual hole EGB is:

$$\sigma_{sr} = \sigma_0 \left[\left(\frac{r}{r_0} \right)^{-\alpha} + \left(\frac{a-r}{r_0} \right)^{-\alpha} \right] \quad (5)$$

where σ_{sr} is the peak stress under the action of a two-hole blast.

The tensile stress at any position in the direction of energy-gathering is:

$$\sigma_t = \frac{\mu}{1 - \mu} \sigma_{sr} \quad (6)$$

When the tensile stress resulting from the overlapping of stress waves at the midpoint in the direction of dual hole energy accumulation reaches the ultimate strength of the fragile tie rod, a critical failure point is reached, leading to rupture of the rod and connection of the two holes. In case the combined stress wave from the two holes remains below the ultimate tensile strength of the rod at the midpoint, the fissures between the two holes remain unconnected. However, if the superimposed stress wave from the two holes exceeds the ultimate tensile strength of the rod at the midpoint, the fissures between the two holes will be connected, albeit resulting in energy wastage. When the tensile stress resulting from the superposition of stress waves at the midpoint position in the direction of dual hole energy

accumulation equals the ultimate strength of the brittle tie rod, the rod experiences critical fracture, leading to the connection of the two holes. This signifies the optimal spacing between the two holes. The optimal spacing can be deduced by employing Eq. (5):

$$a = r_0 \left(\frac{2\mu\sigma_0}{\sigma_T(1-\mu)} \right)^{\frac{1}{a}} \tag{7}$$

By substituting the blasting parameters into the theoretical formula, the optimal distance between two holes under different energy-gathering coefficients can be obtained as a function of the diameter of the charge, as shown in Fig. 5:

As illustrated in Fig. 5, the optimal spacing between two holes exhibits a positive correlation with the energy-gathering coefficient. However, the rate of change is relatively gradual. The optimal spacing between two holes undergoes an upward trend as the explosive diameter increases, with a slower growth rate in the initial phase and a subsequently accelerated growth rate.

2.3 Analysis of Damage of EGB

Supposing the total count of parallel brittle tie rods linking the two holes is denoted as N , the degree of damage to the rock mass situated between the two holes can be defined as the ratio of the fractured rods to the total number of rods. If the count of fractured rods is denoted as ξ , then: $D = \xi/N$.

According to the mechanical balance conditions are available:

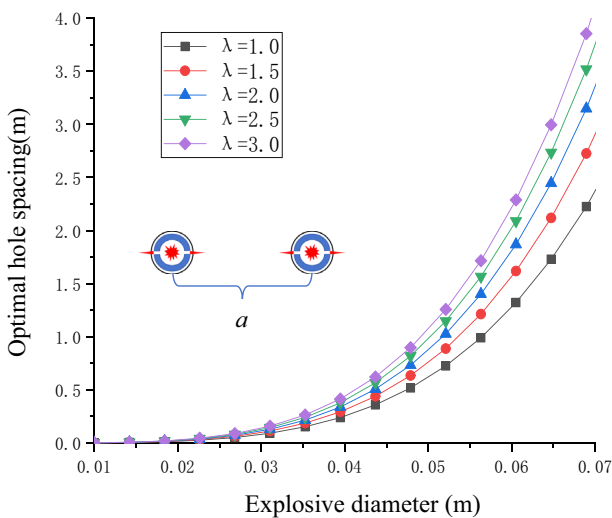


Fig. 5 Curve of optimal duplex spacing with charge diameter under different gather-energy-gathering coefficients

$$F = \sum_{\xi+1}^N k\xi/N = k\xi(1-D) \tag{8}$$

Due to the fact that the specific quantity of rods cannot be accurately measured, if the strength density function of the constructed members is $\theta(\sigma_T)$, then $\theta(\sigma_T)d\sigma$ is the proportion of the number of members with fracture strength within the interval $[\sigma_T, \sigma_T + d\sigma]$. Therefore, Eq. (8) can be transformed into:

$$F = k\xi \left[1 - \int_0^{k\xi} \theta(\sigma_T)d\sigma \right] \tag{9}$$

Then to the damage variable expression:

$$D = \int_0^{k\xi} \theta(\sigma_T)d\sigma \tag{10}$$

Research has shown that the strength of rock elements follows the Weibull function distribution, and the density function is:

$$\theta(f) = \frac{m}{\sigma_T} \left(\frac{f}{\sigma_T} \right)^{m-1} \exp \left[- \left(\frac{f}{\sigma_T} \right)^m \right] \tag{11}$$

Among:

$$m = \ln^{-1} \left(\frac{E\varepsilon_{\max}}{\sigma_{\max}} \right) \tag{12}$$

Put formula (11) into formula (10), integrate after get:

$$D = 1 - \exp \left[- \left(\frac{f}{\sigma_T} \right)^m \right] \tag{13}$$

If $f = \sigma_t(r)$, the damage value at the distance r from the explosion center is:

$$D(r) = 1 - \exp \left[- \left(\frac{\sigma_t(r)}{\sigma_T} \right)^m \right] \tag{14}$$

To study the relationship between the damage value at any point in the direction of energy-gathering and the distance between detonation centers under different energy-gathering coefficients, the blasting parameters under the condition of an explosive diameter of 70 mm were substituted into formula (14), and the curve was fitted using plotting software as follows:

When the damage coefficient (D) of the rock mass reaches 1, it signifies complete fracture. Consequently, when the damage coefficient of the rock mass is 1, the crack length at this time represents the extension length of the main crack. Where D is Damage coefficient of rock mass. As demonstrated in Fig. 6, the extension length of the primary crack escalates proportionally with an increase in the energy-gathering parameter.

Simultaneously, the degree of damage experiences a decline as the distance between the blasting centers widens. The trend of attenuation follows a pattern of initially slower rates, followed by a more rapid decline, culminating in subsequently slower rates.

3 Numerical Analysis of Double-Hole EGB

3.1 Numerical Model

This chapter employs LS-DYNA software to conduct numerical analysis on the dynamics of blasting, three varieties of double hole EGB models were constructed. These models had hole spacings of 1 m, 2 m, and 3 m, respectively, as visually represented in Fig. 7. The diameter of the blasting hole measures 90 mm, while the explosive possesses a diameter of 70 mm. Additionally, the energy-gathering tube has a thickness of 10 mm, with a 10 mm width incision, and a non-reflective boundary (Table 1).

Since the rock is a brittle material, the HJC constitutive model (HJC is a model for describing the ontological relationship between the stress and strain responses of materials subjected to the high temperatures of an explosion) is selected for this simulation, and the explosive is described by the MAT_HIGH_EXPLOSIVE model and the JWL equation of state (JWL is a one-dimensional strain-energy equation that simulates the change between strain energy and elastic energy of a material under load):

$$p = A\left(1 - \frac{\omega}{R_1 V}\right)e^{-R_1 V} + B\left(1 - \frac{\omega}{R_2 V}\right)e^{-R_2 V} + \frac{\omega E_0}{V} \quad (15)$$

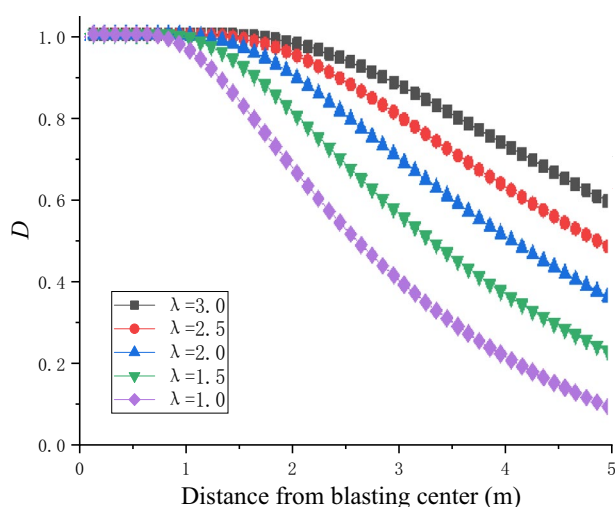


Fig. 6 Change curve of damage distance with burst core distance under different energy-gathering coefficients

where p is the detonation pressure; E_0 is the internal energy per unit volume; V is the relative volume; A , B , R_1 , R_2 and ω are material constants, see Table 2, Table 3 and Table 4 for specific parameters:

3.2 Numerical Results Analysis

By observing the decay pattern of stress waves in blasting, it is apparent that these waves rapidly diminish during propagation. As the attenuated stress fails to further expand the rock cracks, the expansion of the cracks comes to a halt. To ensure optimal roof cutting and pressure relief effects, maintaining crack continuity between blasting holes becomes particularly critical. If the spacing between EGB holes is excessively small, although the cracks connecting the two holes may be established, the surplus energy generated by the blasting would inflict excessive damage upon the surrounding rock. This would also lead to material wastage and an increase in construction volume. On the other hand, if the spacing between EGB holes is too large and the attenuation of blasting stress waves is insufficient to penetrate the cracks between the holes, it would negatively impact the cutting effect. Therefore, to effectively and reasonably harness the energy generated by blasting, it is imperative to optimize the spacing between blasting holes.

To achieve this optimization, three hole spacing schemes of 1 m, 2 m, and 3 m were designed. Furthermore, model layout A, B, C, D, and E measurement points were arranged, with measurement point E residing at the midpoint between the two holes, as depicted in Fig. 8.

3.2.1 Analysis of effective stress distribution in EGB patterns with varying hole spacing

Figure 9 illustrates the distribution of effective stress during double hole EGB, where the distance between the holes spans 1 m. At $t = 25 \mu\text{s}$, the pinnacle of effective stress amounts to an impressive 65.81 MPa. Notably, this high stress region encompasses the vicinity of the double blasting holes, inducing the formation of crushing zones. Furthermore, horizontal cracks materialize along the direction of energy accumulation. As time elapses, specifically at $t = 100 \mu\text{s}$, the maximum effective stress diminishes to a modest 36.46 MPa. It is worth mentioning that the stacking of stress waves between the two holes commences during this interval. Consequently, the primary crack expansively progresses horizontally. However, owing to the confluence of stress waves, excessive energy propels the crack growth on the side devoid of energy accumulation. Upon reaching $t = 200 \mu\text{s}$, the effective stress dissipates to 22.29 MPa. Remarkably, the cracks aligning with the direction of energy accumulation interconnect between the pores, while those on the non-energy accumulating side persist in their expansion.

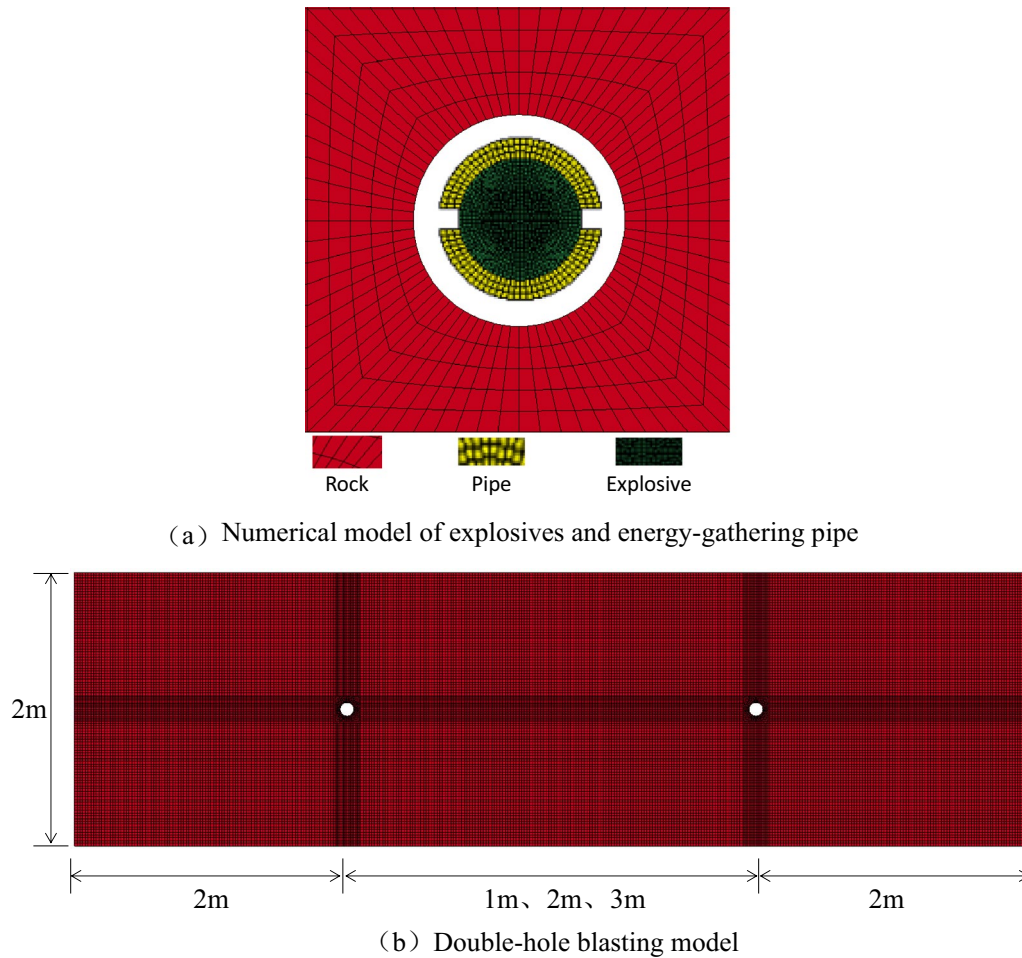


Fig. 7 Numerical geometric calculation model. a Numerical model of explosives and energy-gathering pipe. b Double-hole blasting model

Table 1 Blasting parameters

ρ_e (kg·m ⁻³)	V_{max} (m·s ⁻¹)	σ_T (MPa)	d_b (mm)	n	μ
1180	5122	8.2	90	10	0.3

Finally, at $t = 300 \mu s$, the gradual attenuation of effective stress culminates in a value of 21.79 MPa. In this quiescent state, the crack ceases its relentless expansion. Notably, the

energy accumulating side crack reaches an extension length of 1.2 m, while the non-energy accumulating side crack extends up to 0.7 m.

Figure 10 illustrates the effective stress resulting from double hole EGB, with a spacing of 2 m. When $t = 25 \mu s$, the maximum effective stress is recorded at 62.20 MPa. Notably, crushing zones can be observed surrounding the double blasting holes, while horizontal cracks manifest in the direction of horizontal energy accumulation. As time

Table 2 Physical and mechanical parameters of explosives

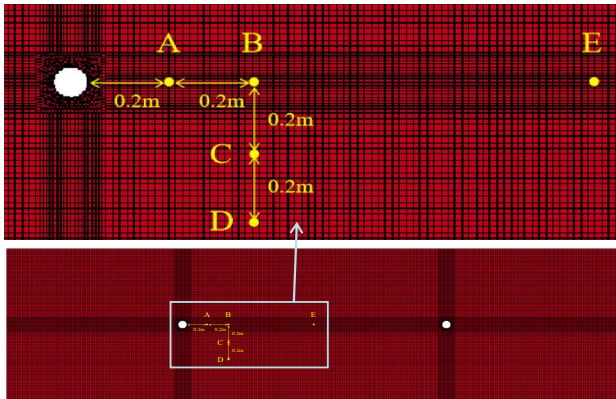
ρ_e (kg·m ⁻³)	C_d (m·s ⁻¹)	A_1 (GPa)	B_2 (GPa)	R_1	R_2	ω	P_{CJ} (GPa)	E_0 (GPa)
1180	5122	276.2	8.44	5.2	2.1	0.5	9.53	3.87

Table 3 Physical and mechanical parameters of the rock

ρ_e (kg·m ⁻³)	f_c (MPa)	A	B	C	S_{max}	G (GPa)	T (MPa)	D_1	D_2
2600	60	0.28	2.5	0.00186	5	28.7	12.2	0.04	1
FS	μ_{lock}	P_{crush}	P_{lock}	μ_{crush}	K_1	K_2	K_3	EF_{min}	N
0.035	0.012	51	1.2	0.00162	12	25	42	0.01	0.79

Table 4 Physical and mechanical parameters of blasting energy-gathering pipe

d_w (mm)	d_n (mm)	b (mm)	ρ (kg·m ⁻³)	μ	E (GPa)	f_t (MPa)	f_y (MPa)
50	70	10	1380	0.32	8.6	64	75

**Fig. 8** Arrangement diagram of double-hole blasting monitoring point

progresses to $t = 100 \mu\text{s}$, the maximum effective stress attenuation is measured at 41 MPa, surpassing the effective stress observed at a hole spacing of 1 m. During this stage, the primary crack continues its expansion horizontally. Upon reaching $t = 200 \mu\text{s}$, the effective stress attenuation stands at 30.99 MPa, with further expansion seen in the cracks between the pores in the direction of energy accumulation. Convergence and overlap of stress waves from the two pores lead to the appearance of cracks on the non-energy accumulation side. Finally, when $t = 300 \mu\text{s}$, the maximum effective stress attenuation reaches 26.59 MPa. It is at this juncture that crack expansion halts, and the energy accumulating side crack extends up to a maximum length of 1.2 m, while the non-energy-gathering side crack experiences marginal expansion, with a maximum length of only 0.1 m. This discrepancy indicates minimal energy wastage.

The numerical analysis of double hole EGB, this time with a hole spacing of 3 m, is presented in Fig. 11. At $t = 25 \mu\text{s}$, the maximum effective stress value is recorded at 62.68 MPa, mirroring the presence of crushing zones surrounding the double blasting holes and the emergence of horizontal cracks in the direction of horizontal energy accumulation. As time progresses to $t = 100 \mu\text{s}$, the maximum effective stress escalates to 95.52 MPa, surpassing the peak value attained when the hole spacing is 1 m or 2 m. This observation signifies that, in tandem, larger hole spacings yield higher maximum effective stress values. At $t = 200 \mu\text{s}$, the effective stress attenuation equates to 51.44 MPa, accompanied by continued expansion of cracks between the pores in the direction of energy accumulation. Upon reaching $t = 300 \mu\text{s}$, the maximum effective stress attenuation stands

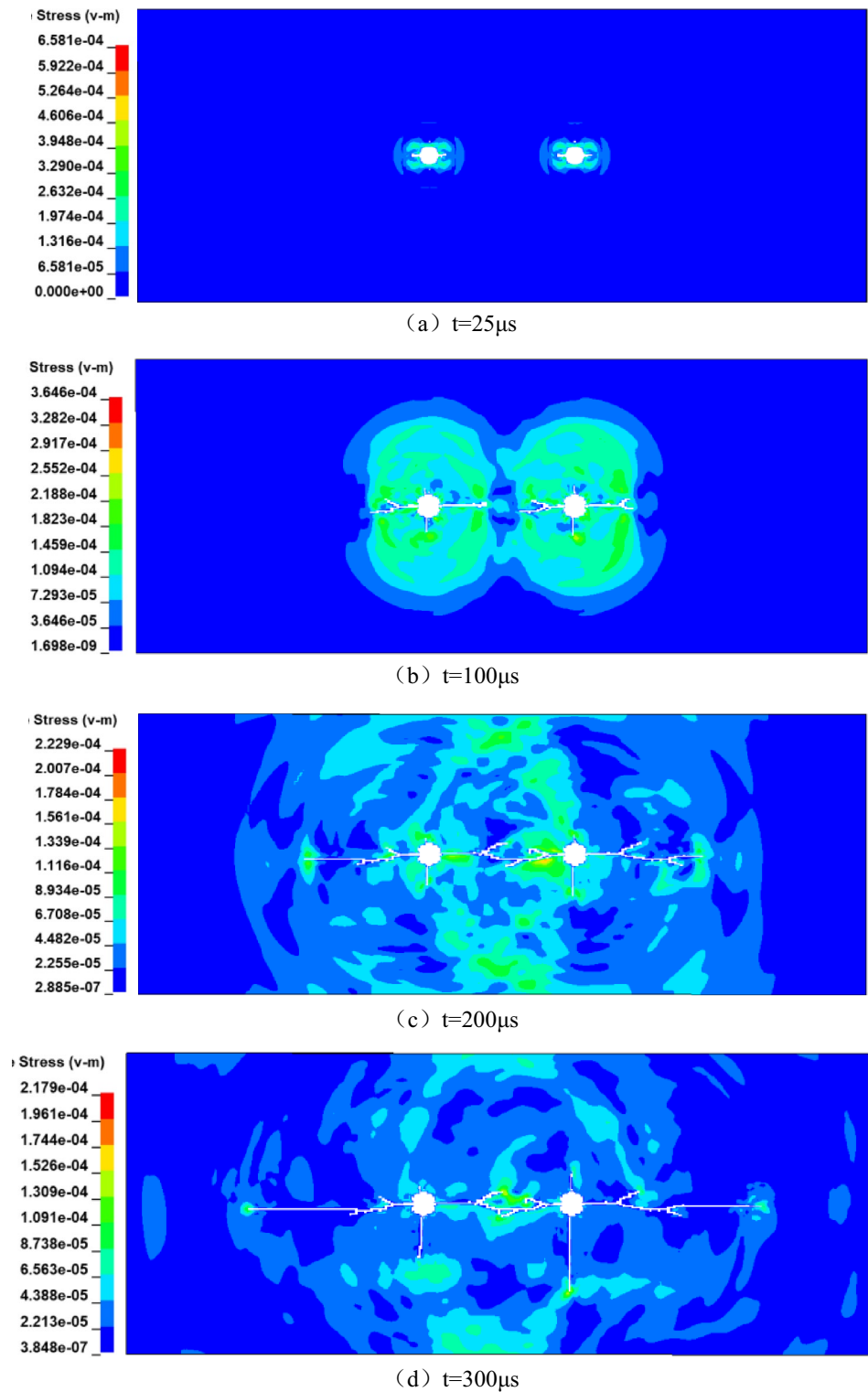
at 34.88 MPa, while the stress waves generated by the two holes commence convergence. However, the resultant stress, post-convergence and superposition, lacks the strength required for sustaining crack propagation. Consequently, crack expansion halts at this stage. Only transverse cracks emerge on the energy accumulating side, with a maximum expansion length of 1.2 m. Conversely, no cracks form on the non-energy accumulating side. This outcome indicates an absence of energy wastage at this particular point.

3.2.2 (2) Effective stress curve analysis of EGB at different hole spacing, as shown in Fig. 12

The time history curve of effective stress for each measuring point in the double hole EGB, with a 1 m spacing between holes, is presented in Fig. 12 (a). By comparing the effective stress curves at measurement points A and B, it becomes apparent that the stress wave propagates from point A to point B, with an attenuation of approximately 40 MPa. This observation suggests that as the propagation distance increases, the peak stress experiences a diminishing trend. On further comparison, the effective stress curves at measurement points B, C, and D reveal an attenuation pattern in the non-energy accumulation direction. An analysis of the effective stress curve at point A indicates that at $t = 70 \mu\text{s}$, there is a noticeable characteristic of increased effective stress, indicating that the stress wave in the right hole has already propagated to point A, resulting in an augmented attenuated stress value. Furthermore, based on the effective stress curve at point E, at $t = 52 \mu\text{s}$, the stress waves from both holes propagate to the midpoint, leading to stress superposition. The maximum effective stress reaches 90 MPa, which closely approximates the peak effective stress at point A near the hole opening. This finding suggests that the spacing of 1 m between the holes is too close, leading to significant energy waste.

Figure 12 (b) depicts the time history curve of effective stress for each measuring point in the double hole EGB, with a 2 m spacing. From the figure, it is evident that the secondary increase in effective stress values at each measuring point weakens. The maximum value of this secondary increase is only 40 MPa, indicating a diminished influence of stress wave superposition and a reduction in energy waste. Additionally, the effective stress curve at point E showcases that at $t = 110 \mu\text{s}$, the stress waves from both holes propagate to the midpoint, resulting in stress superposition. The maximum effective stress reaches 50 MPa, which is a decrease of 40 MPa in comparison to the 1 m hole spacing. This further validates the reduction in wastage of blasting energy.

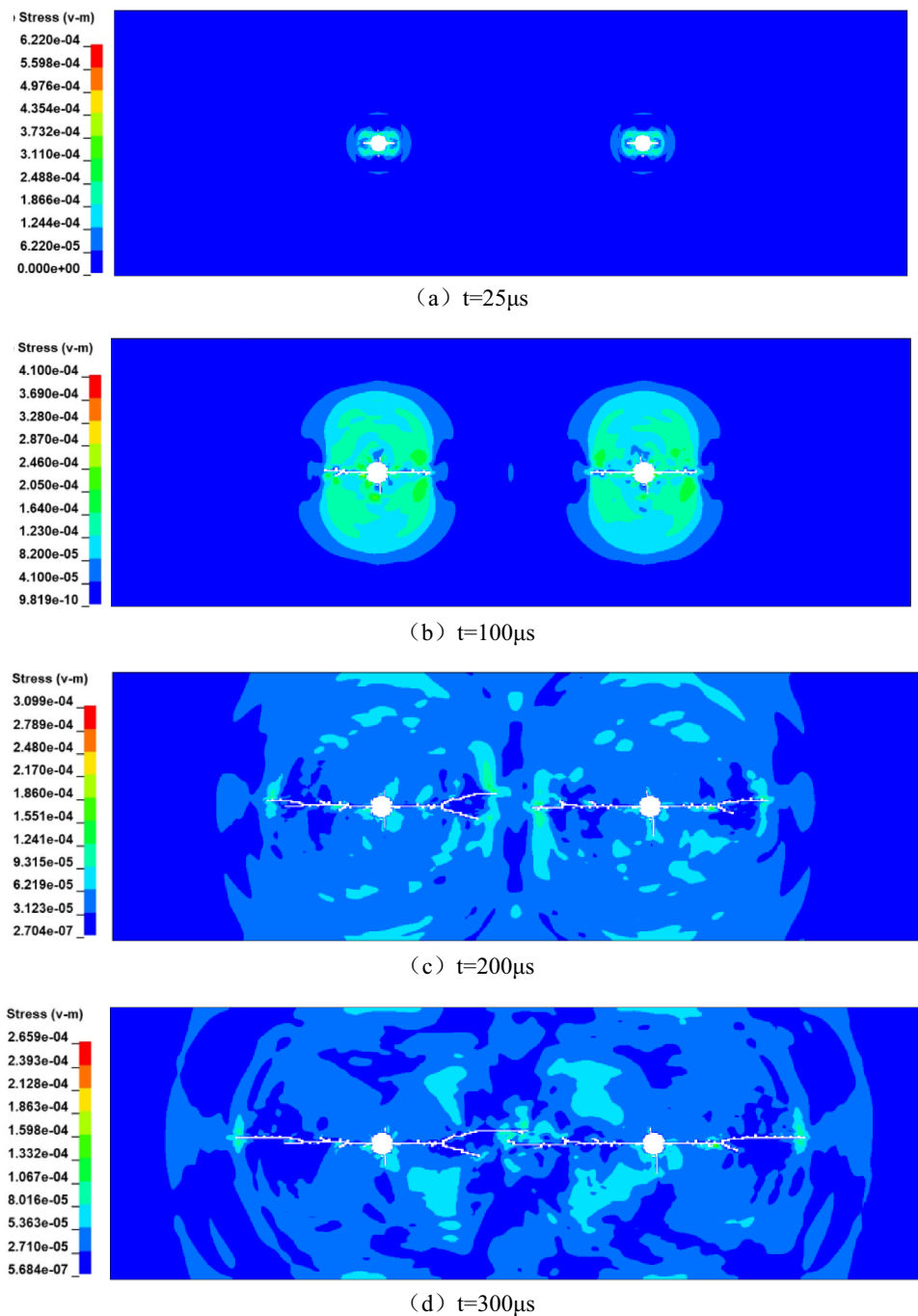
Fig. 9 Cloud diagram of effective stress of EGB with hole spacing of 1 m (10^{-5} MPa). **a** $t=25 \mu\text{s}$. **b** $t=100 \mu\text{s}$. **c** $t=200 \mu\text{s}$. **d** $t=300 \mu\text{s}$



The time history curve depicting the effective stress of each measuring point in the double hole EGB, with a spacing of 3 m, is illustrated in Fig. 12 (c). As observed in the diagram, the secondary increment in effective stress values at each measuring point weakens subsequently. Moreover,

the maximum value of the secondary stress increase is less than 40 MPa, affirming a reduction in the superposition of blasting stress waves and a decrease in energy dissipation. Furthermore, from the effective stress curve of point E, it can be discerned that at $t=150 \mu\text{s}$, the stress waves from

Fig. 10 Cloud diagram of effective stress of EGB with hole spacing of 2 m (10^{-5} MPa). **a** $t = 25 \mu\text{s}$. **b** $t = 100 \mu\text{s}$. **c** $t = 200 \mu\text{s}$. **d** $t = 300 \mu\text{s}$



both holes propagate towards the midpoint, resulting in stress superposition. This yields a maximum effective stress of 30 MPa, which is a reduction of 60 MPa compared to the case where the hole spacing is 1 m. This once again validates the mitigation of energy wastage during blasting.

Based on the aforementioned analysis, it can be deduced that when the spacing between holes is 1 m, despite enabling the connection of cracks between the holes, the proximity leads to substantial energy loss. Conversely, when the spacing is set at 3 m, although there is no energy waste,

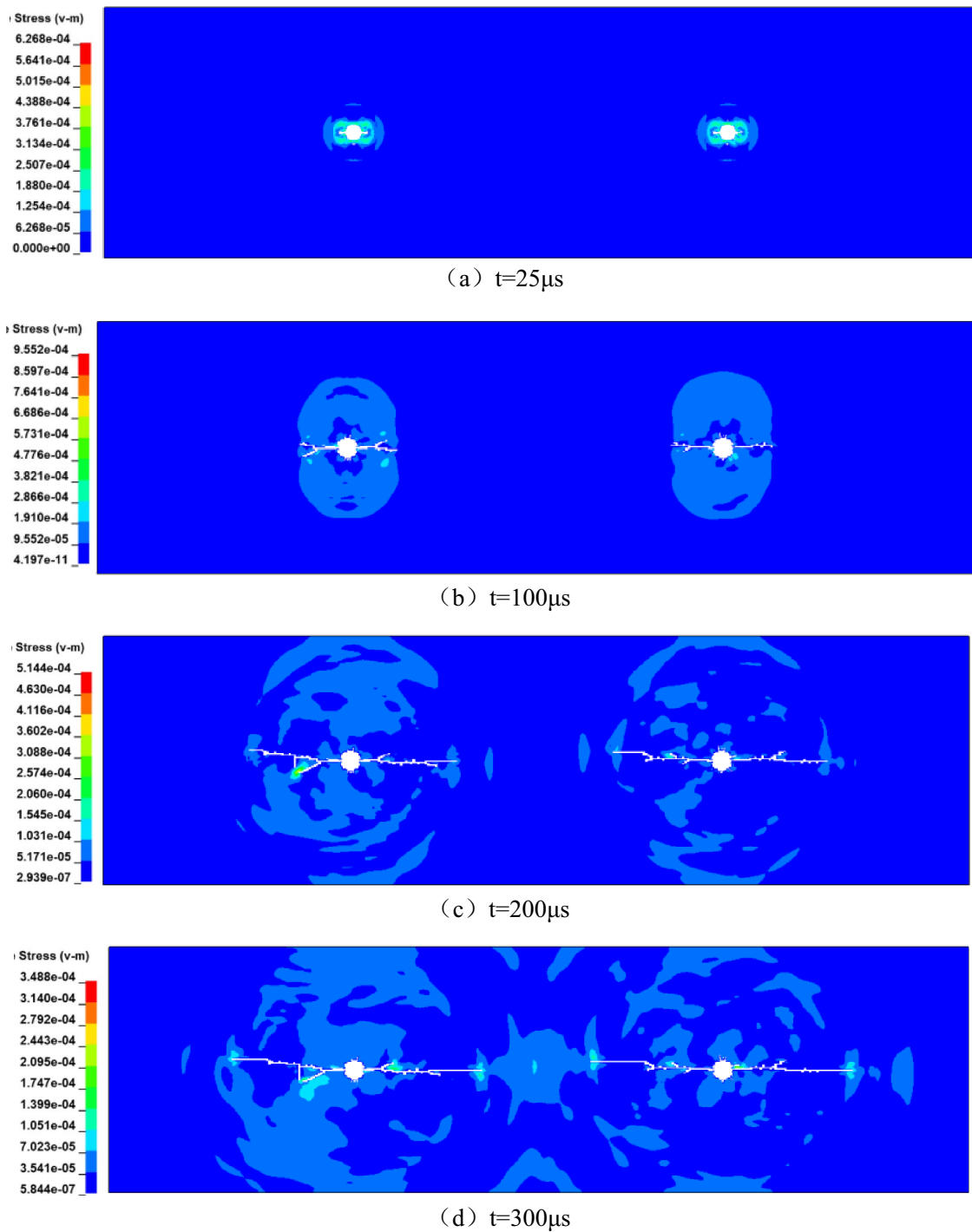
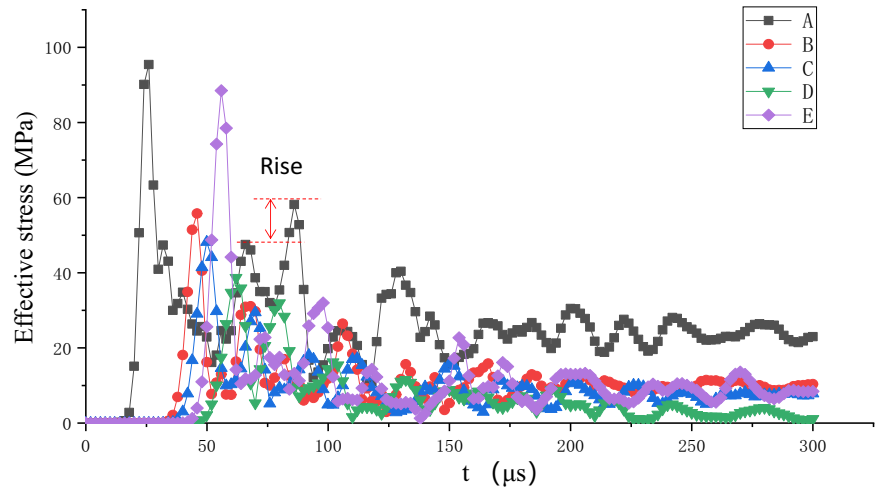


Fig. 11 Cloud diagram of effective stress of EGB with hole spacing of 3 m (10^{-5} MPa). **a** $t=25\ \mu\text{s}$. **b** $t=100\ \mu\text{s}$. **c** $t=200\ \mu\text{s}$. **d** $t=300\ \mu\text{s}$

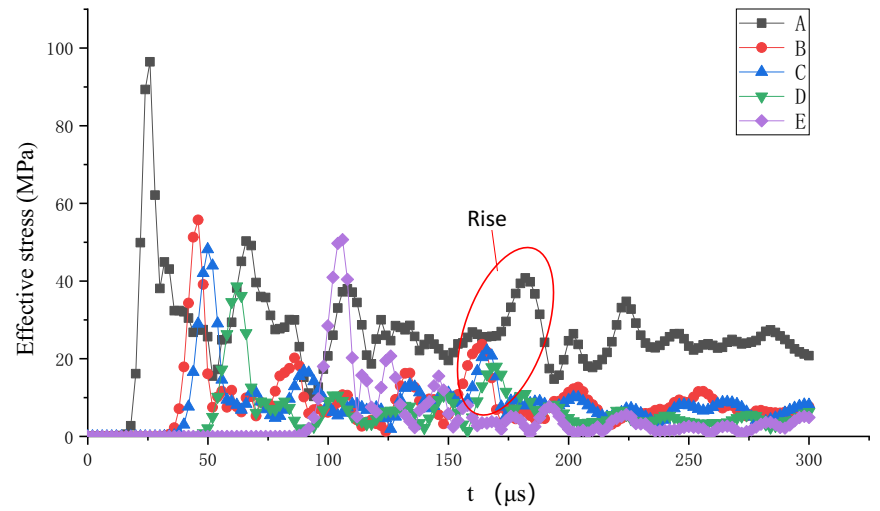
the cracks between the holes fail to align, impeding the attainment of optimal cutting. Therefore, a spacing of 2 m between EGB holes emerges as the ideal choice. This

arrangement not only ensures the uninterrupted propagation of cracks but also minimizes energy dissipation while significantly reducing damage on the non-energy accumulation side.

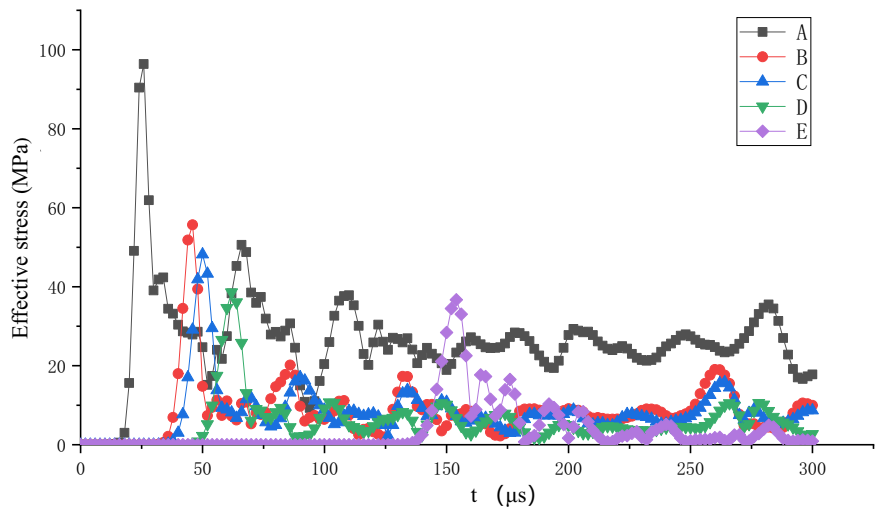
Fig.12 Effective stress curve EGB with different hole spacing. a 1 m. b 2 m. c 3 m



(a) 1m



(b) 2m



(c) 3m

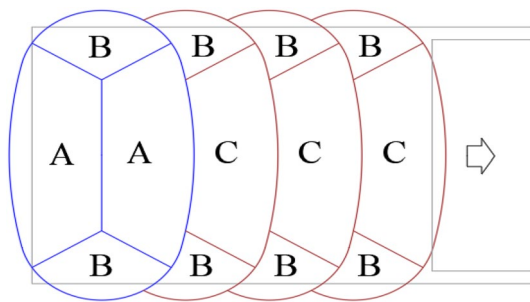


Fig. 13 Schematic diagram of stope overburden roof collapse pattern

4 Analysis of the Surrounding Rock Pressure Relief Mechanism

After the extraction of coal seams, the original stress structure of the rock layers undergoes a significant change, leading to a loss of support from the coal mass in the overlying rock layers. Initially, the immediate upper roof collapses, whereas the fundamental roof rock layer, being thicker and possessing greater strength, resists collapse as a crucial layer. The mining process pushes the working face forward, gradually expanding its exposed area. Once the suspended roof reaches its limit, fractures occur, resulting in the formation of two collapsing rock blocks, namely A and B, as illustrated in Fig. 13.

The initial collapse of the rock layer’s roof alters the stress distribution of the remaining non-collapsed roof. As mining progresses, the length of the suspended roof continues to increase until it reaches its maximum extent, leading to periodic fractures and the creation of rock blocks B and C. The periodic collapse pattern is depicted in Fig. 13. Examining the pressure distribution characteristics in the mining area reveals that the working face experiences the greatest influence from rock blocks A and C, while the surrounding rock of the goaf roadway is primarily affected by rock block B. The extensive cantilever structure of rock block B serves as the primary cause for the heightened stress concentration in the coal pillar. Consequently, the key to controlling the deformation of the surrounding rock in the goaf roadway lies in reducing the length of this cantilever structure.

When the coal seam exhibits a substantial thickness and the immediate roof is relatively thin, the filling degree of gangue within the goaf is diminished post-mining, rendering it arduous to provide effective support for the cantilever structure. Solely the terminal coal pillar receives support, resulting in an elevation of lateral support pressure on the coal pillar, as depicted in Fig. 14 (a). The rupture or sliding of the structure further intensifies the support pressure on the coal pillar’s flank, constituting the principal basis for stress concentration in roadway. By implementing concentrated energy blasting technology to alleviate surrounding rock

pressure, the extensive cantilever structure of the rock layer can be severed, leading to its rapid collapse and expansion into the goaf. This effectively bolsters the overlaying rock strata, mitigating subsidence deformations and subsequently reducing stress concentration in the surrounding rock of roadway, as demonstrated in Fig. 14 (b).

Suppose the average vertical stress of the coal pillar non roof cutting is $\overline{\sigma}_{y1}$, and post-roof cutting is $\overline{\sigma}_{y2}$, with the coal seam thickness labeled is y_1 , the falling zone thickness is y_2 the fracture zone thickness is y_3 , the load on the overlying line of the fracture zone is q_1 , the load on the vertical support line of gangue crushing expansion is q_2 , the load on the lateral support line is q_3 , and the unit weight of the overlying rock is γ , the stress equilibrium conditions of the surrounding rock system prior to roof cutting and pressure relief are as follows:

$$\overline{\sigma}_{y1}x_1 = q_1(x_1 + x_2 + x_3) + y_3(x_1 + x_2 + x_3)\gamma + y_2(2x_1 + 2x_2 + y_2 \tan \theta)\gamma/2 + (S_1 + S_2)\gamma \quad (16)$$

$$\overline{\sigma}_{y2}x_1 = q_1(x_1 + x_2 + x_3) + y_3(x_1 + x_2 + x_3)\gamma + y_2(2x_1 + 2x_2 + y_2 \tan \theta)\gamma/2 - q_2(x_2 - y_2 \tan \theta) - q_3y_2 \sin \theta \quad (17)$$

After roof cutting, the stress exerted on the coal pillar’s flank diminishes as:

$$\Delta\overline{\sigma} = \overline{\sigma}_{y1}x_1 - \overline{\sigma}_{y2}x_1 = (S_1 + S_2)\gamma + q_2(x_2 - y_2 \tan \theta) + q_3y_2 \sin \theta \quad (18)$$

5 Engineering Application

5.1 Project Overview

The 122,108 working face at Caojiatan Coal Mine spans a length of 280 m and stretches for 5910 m along its strike. The mining process employed here is fully mechanized top-coal caving, where coal is mined to a depth of 5.8 m and subsequently caved to a depth of 5–6 m. The coal seam being extracted is the 2–2 seam, which boasts an average thickness of 10.25 m. It has an inclination angle ranging from 0° to 5° and lies buried between 300 and 363 m beneath the surface. The immediate roof comprises fine sandstone with a thickness of 4.92 m, while the main roof consists of medium sandstone measuring 20.4 m in thickness. Due to the large disturbance of the caving mining method and the inherent difficulty in collapsing the thick basic roof, the manifestation of dynamic pressure is particularly pronounced. Furthermore, the presence of the 122,108 goaf and the adjacent 122,106 working face exacerbates this issue, causing significant stress concentration in both the coal pillar and the working face. Consequently, the goaf roadway experiences substantial

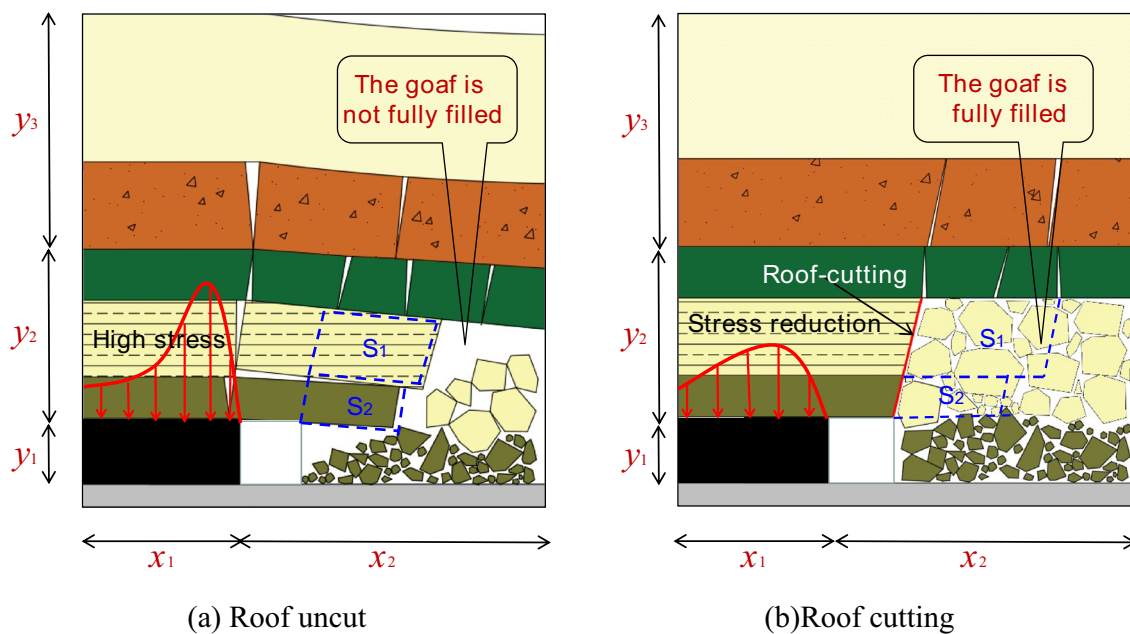


Fig. 14 Principle of roof cutting and pressure relief. **a** Roof uncut. **b** Roof cutting

deformation, especially in the advanced section where the end support is located. Here, the floor heave is particularly severe, reaching a maximum of 800 mm. The extensive ground breaking engineering in the roadway severely hampers the progress of mining operations and scaffolding work. To address the substantial deformation occurring in the roadway, a new technological solutions have been proposed, known as the roof cutting in advance working face, was proposed to mitigate the deformation by preemptively reducing pressure as the roof cutting. A test section for pressure relief is depicted in Fig. 15.

5.2 Design of the Roof-cutting Parameters

The design of EGB involves consideration of various factors such as the impact on seam cutting, roof span falling, and stability of the goaf roadway. It is particularly essential to determine key parameters, including the direction of cutting, angle of cutting seam, height of cutting, spacing of blasting holes, and amount of explosives.

5.2.1 (1) Direction of Roof Cutting

Cutting the roof on both sides of the roadway can reduce stress on both sides. However, the formation of an inverted trapezoidal structure by the roadway renders it comparatively unstable. Additionally, the auxiliary transport roadway 122,106 becomes waterlogged after sustaining damage. Blasting and roof cutting along the side of the coal pillar

may introduce goaf water into the 122,108 working face. Therefore, the direction of the working face for roof cutting in the return air roadway of the 122,108 working face is selected as the roof cutting direction.

5.2.2 (2) Angle of Roof Cutting

To minimize frictional forces on the roadway roof during goaf roof collapse and enhance the support provided by crushed and swollen rocks on the cantilever beam, the cutting joint surface needs to form a specific angle with the horizontal plane. If the cutting angle is excessively large, equal to or exceeding 90° , the roadway roof will experience frictional pressure when the goaf roof sinks, impeding the collapse of the goaf roof and increasing subsidence of the roadway roof and the difficulty of roof support. Furthermore, charging at a large angle becomes exceedingly challenging. Conversely, if the cutting angle is too small, it will result in increased length and volume of the cantilever beam, rendering pressure relief ineffective. Moreover, a small angle increases the difficulty of drilling construction and raises the cost of retaining roadway.

Therefore, selecting an appropriate cutting angle is crucial. Based on the geological conditions of the mine and previous experience in roof cutting engineering, an angle of 60° between the EGB roof cutting angle and the horizontal plane is chosen. At the same time, a non-EGB hole is added, the horizontal angle degree is 50° , to increase the swelling

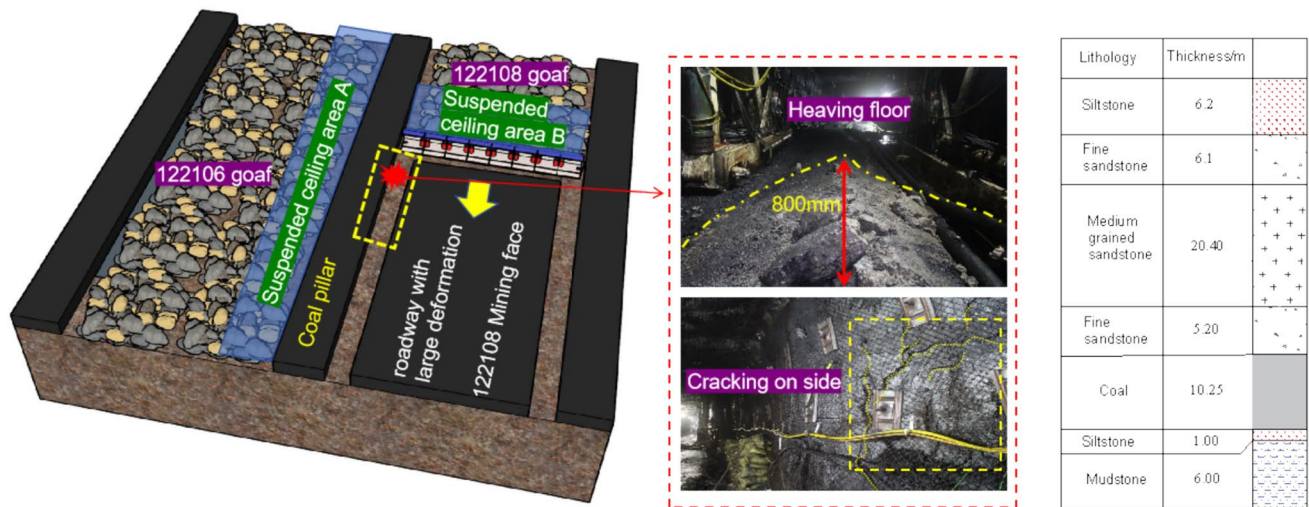


Fig. 15 Schematic diagram of the coal mining face

degree of gangue, to ensure that the broken gangue has a certain supporting effect on the basic top rock layer and collapses smoothly.

5.2.3 (3) Height of roof cutting

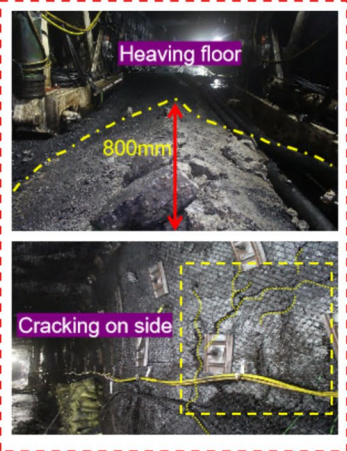
The cutting height must ensure the interruption of the key layer’s cantilever structure while considering parameters such as coal seam mining height, caving height, and crushing expansion coefficient. To support the goaf rock layer with collapsed gangue, it is necessary to fill the goaf with crushed gravel.

Therefore, the cutting height for top coal caving mining can be calculated using the following equation:

$$H_f = (H_m + H_d) / (K - 1) + H_d \tag{19}$$

where H_f is the height of the roof-cutting, H_m is the thickness of coal mining, H_d is the thickness of top coal caving, K is the coefficient of fragmentation and expansion of gangue.

The coal seam thickness in the operational area ranges between 9.75 and 11.2 m, with an average thickness of 10.25 m. There is a remaining bottom coal layer measuring 0.5 m. The extracted coal seam has a thickness of 9.75 m, while the top coal is approximately 5 m thick. The coefficient of fragmentation and expansion is determined to be 1.38. By substituting these parameters into theoretical formula 19, the cutting height can be calculated to be 30.6 m. Taking a cutting angle of 60°, the length of the cutting hole can be calculated in reverse to be 35.3 m. However, based on previous experience, it is known that when the cutting length reaches 0.9 times the theoretically calculated length, the uncut upper rock mass can collapse on its own. Therefore, the engineering design EGB hole



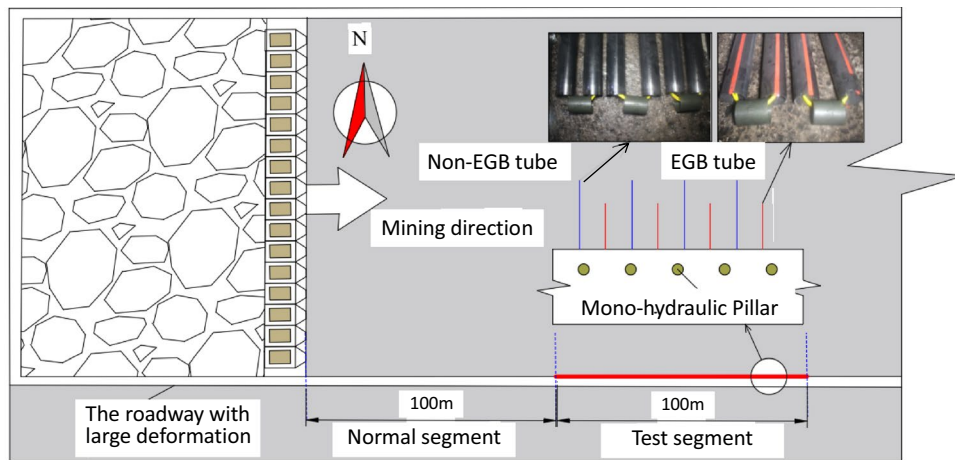
length is set at 32 m. To ensure a consistent cutting height, the design non-EGB hole length is set at 33 m.

5.2.4 (4) Hole Spacing and Dosage

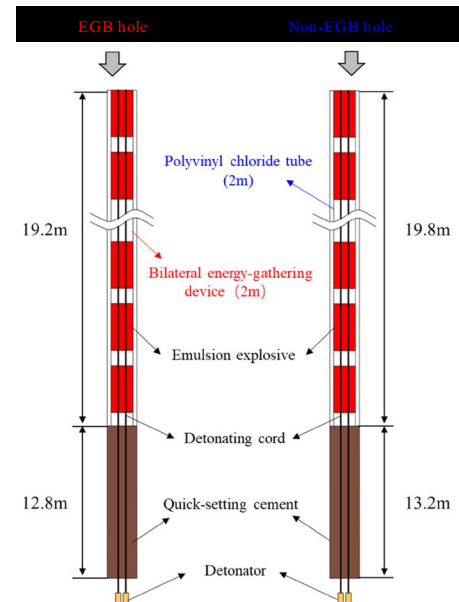
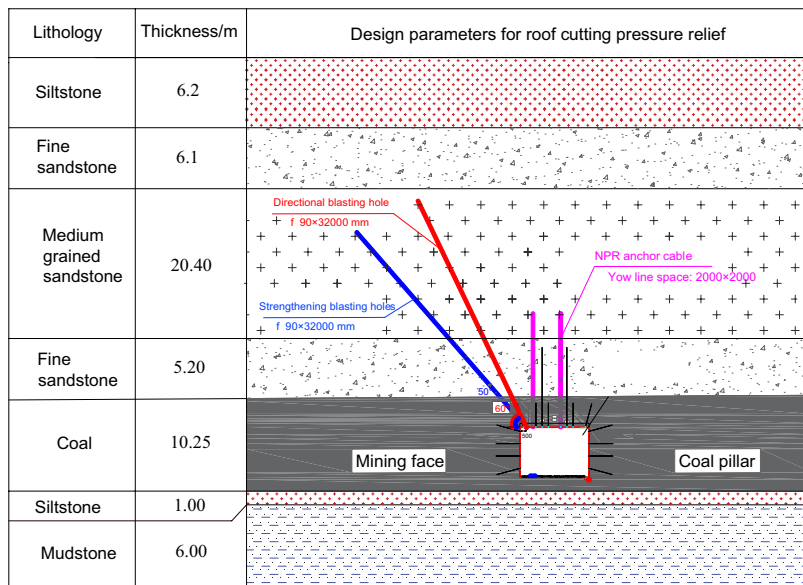
Regarding hole spacing and charge quantity, after conducting a comprehensive analysis of the geological conditions in the working area, the location of the drilling within the rock strata, and the results of theoretical analysis, a combination blasting method is adopted that involves directional cutting and non-directional pressure relief towards the side of the roadway. Each group consists of a 60° EGB hole measuring 32 m and a 50° non-EGB hole measuring 33 m. The spacing between EGB holes is set at 2 m, and a non-EGB hole is added between the two EGB holes to enhance the blasting force and accelerate the expansion of the roof fracture. The charging coefficient is determined to be 0.6, and the blasting employs three-level coal mine emulsion explosives with a blast hole diameter of 90 mm. The blasting technique used is forward blasting, with the bottom of the hole filled with explosives, occupying a length that is 0.6 times the hole depth. The outer opening of the hole is sealed with mud, and rapid-setting cement is used to seal the hole, with a length that is 0.4 times the hole depth. The charging structure is depicted in Fig. 16.

5.3 Monitoring Protocol

To examine the impact of roof cutting and pressure relief, it is imperative to monitor the deformation, support pressure, and coal stress of the roadway. To assess the effect of roof cutting and pressure relief, an analysis of the monitoring data is necessary. The hydraulic support monitoring on the



(a) Layout plan of blasting hole and hydraulic unit



(b) Sectional drawing of blasting hole layout and charging structure

Fig. 16 Layout of working face and borehole histogram. **a** Layout plan of blasting hole and hydraulic unit. **b** Sectional drawing of blasting hole layout and charging structure

working face employs the original monitoring equipment provided by the mining party, with each advance support outfitted with a pressure monitor. Deformation measurements of the roadway roof and floor are conducted at the advance support, while coal stress monitoring takes place on both the coal pillar side and the working face side of the roadway. The layout of the monitoring points can be observed in Fig. 17.

5.4 Results and Analysis

5.4.1 Support Pressure Analysis

To investigate the changes in pressure exerted by the leading support (roadway position) in the working face due to roof cutting pressure relief, a comparative analysis was performed between the pressure of the normal segment and test segment, in Fig. 18. From Fig. 18(a), it is apparent that

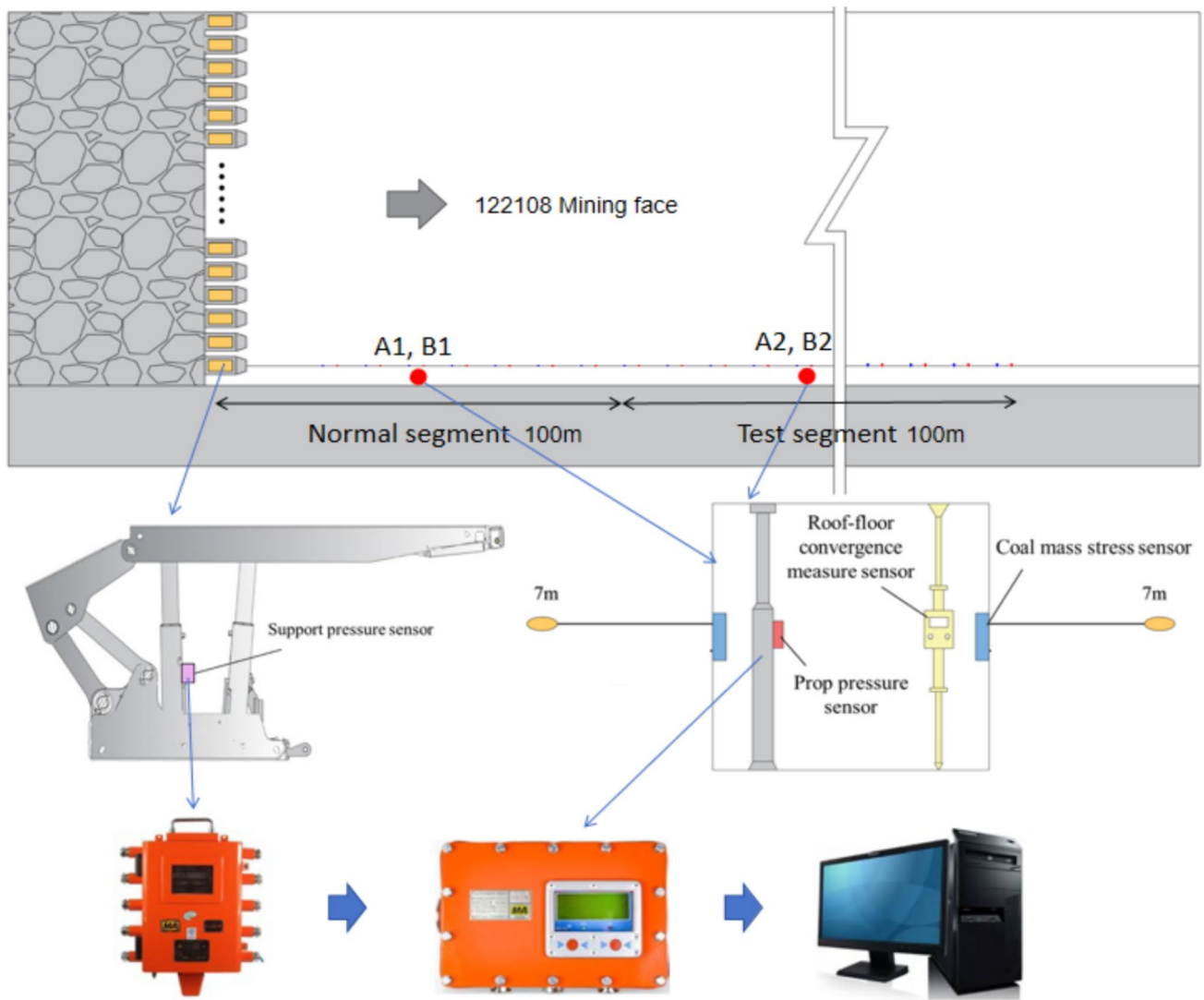
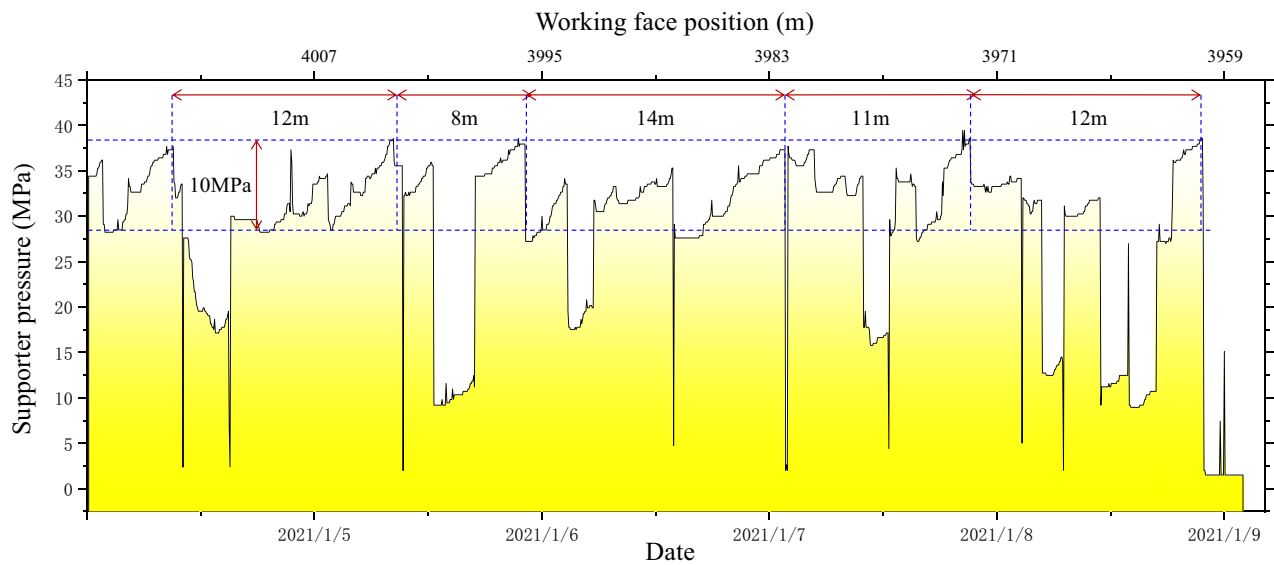


Fig. 17 Schematic diagram of monitoring system

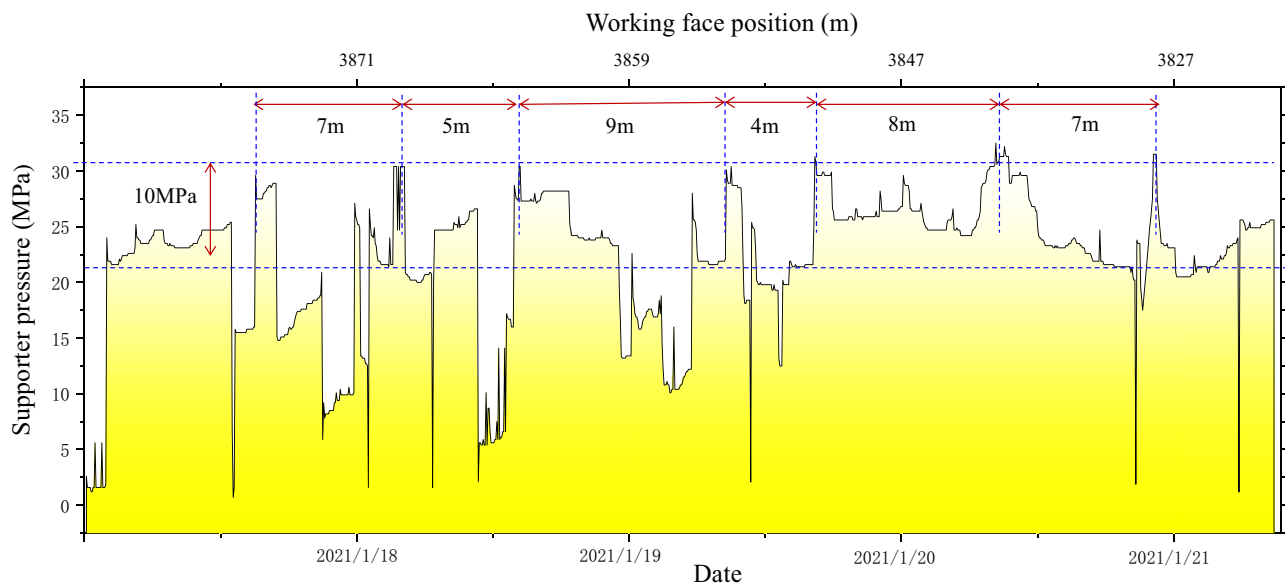
in the normal segment, the average pressure of the leading bracket stood at 27 MPa, with a peak pressure of 37 MPa. The pressure interval ranged from 8 to 14 m, with an average pressure interval of 11.4 m. Turning to Fig. 18(b), it is evident that the average pressure of the leading bracket in the test segment recorded 22 MPa, accompanied by a peak pressure of 32 MPa, representing reductions of 18.5% and 13.5% respectively when compared to the uncut section. The average pressure interval is 6.7 m, a 41% decrease in comparison to the uncut portion.

5.4.2 Surrounding Rock Stress

Monitoring the stress levels of coal involves inserting a flexible detection unit into a borehole and subsequently injecting fluid to expand and fully engage with the coal. As the stress within the coal mass fluctuates, so does the pressure within the injection detection unit. By measuring the variation in pressure along the borehole wall through hydraulic means, one can discern the trends in coal stress fluctuations. To examine the patterns of stress variation within the coal mass prior to roof cutting and within the



(a) Normal segment



(b) Test segment

Fig. 18 Schematic diagram of monitoring system. **a** Normal segment. **b** Test segment

experimental zone, stress variation curves are plotted for different positions within the coal mass. Figure 19 illustrates the stress variation curve on the side of the working face. In the normal segment, the initial stable stress value on the coal pillar side is recorded as 2.8 MPa. Once located 45 m away from the working face, the stress begins

to rise, indicating an approximate range of advanced stress influence is 45 m. Eventually, the stress value escalates to approximately 7.81 MPa, yielding a stress concentration coefficient of 2.79. Within the experimental section, the stress within the coal mass reaches a maximum of 5.72, accompanied by a stress concentration coefficient of 2.04,

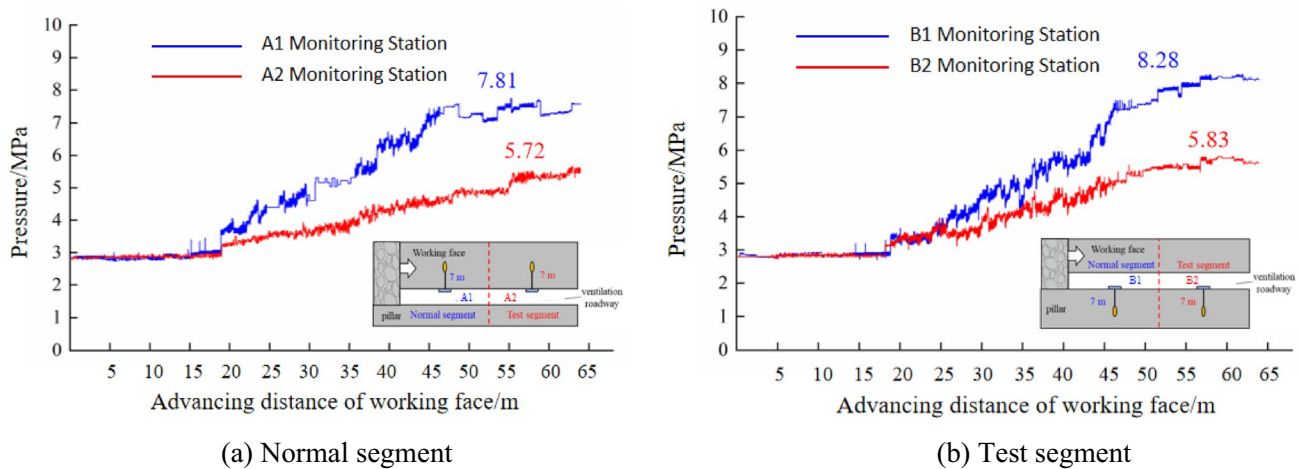


Fig. 19 Coal mass stress monitoring (Yang et al. 2023). **a** Normal segment. **b** Test segment

representing a 26.7% decrease compared to pre-cutting conditions. Likewise, in the normal segment, the stress value on the coal pillar side rises to 8.28 MPa, yielding a stress concentration coefficient of 2.96. In the experimental section, the stress value on the coal pillar side ultimately increases to 5.83 MPa, resulting in a stress concentration coefficient of 2.08, a decrease of 29.6% when compared to normal segment conditions.

5.4.3 Deformation Analysis

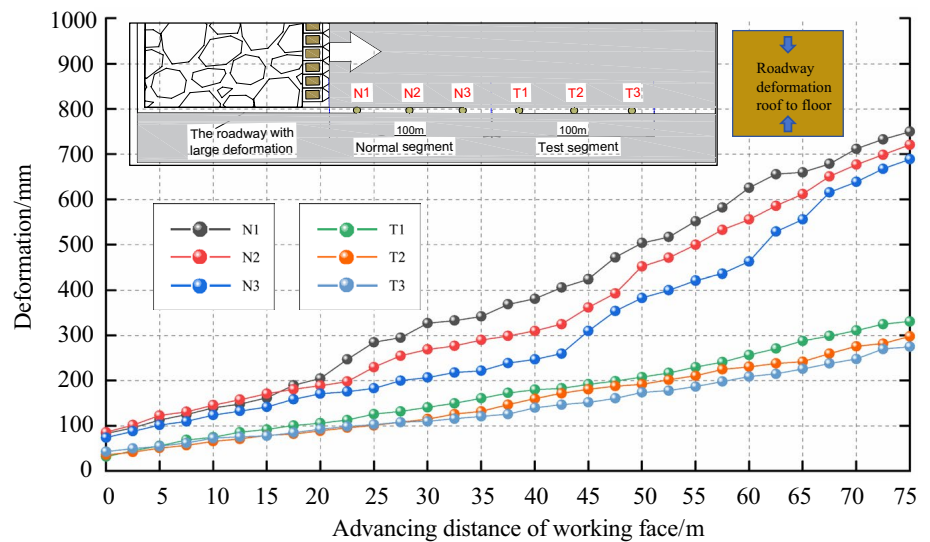
Comparison and analysis of deformation at measurement stations N1, N2, N3 (normal section) and T1, T2, T3 (test section) in Fig. 20. At a distance of 75 m in front of the measurement station, when the working face is excavated, the measurement sensor records the changes in monitoring data at each measurement station. A comparison of deformation changes in the normal section reveals that the deformation speed and magnitude in the test section are substantially lower. Furthermore, as the working face approaches the measurement station, the average convergence values of the top and bottom plates at the three measurement stations in the normal section amount to 720 mm, whereas the average convergence values of the top plates at the three measurement stations in the experimental section are 301.3 mm. This represents a decrease of 58.2%. It can be inferred that the utilization of the EGB method not only significantly reduces road maintenance workload and costs, but also contributes to ensuring road safety.

6 Conclusion

(1) This article delves into the intricacies of directional fracturing technology in EGB. The energy is released through a shaped charge tube device, creating directional cracks in the rock. Drawing upon the theory of parallel rod fracture, a mechanical model is established for EGB and the expansion mechanism of cracks in a fixed direction is analyzed. By considering stress superposition, the analytical formula for the optimal spacing between double holes is solved. Additionally, the relationship between damage is analyzed, variations in energy accumulation coefficient, distance from blast centre, and the diameter of the explosive. The research unveils a positive correlation between the optimal distance between double holes, the degree of damage, the coefficient of energy accumulation, and the explosive diameter. Conversely, there exists a negative correlation between the degree of damage and the distance from blast centre.

(2) This study used numerical simulation to study the differences in EGB with different hole spacing, and analyzed the optimal spacing of dual hole EGB. The findings demonstrate that if the distance between the two holes in the EGB is too close, the cracks can expand in a non-energy-gathering direction due to stress superposition. Conversely, if the distance between the holes is too far, the superimposed stress fails to reach the fracture strength of the rock microelements, impeding double hole crack penetration. Both numerical analysis and theoretical analysis conclusively establish that the optimal hole spacing is 2 m, which supports the

Fig. 20 Deformation of surrounding rock of roadway (Yang et al. 2023)



theoretical analysis results. It has also been proven that EGB can protect rocks in non-shaped charge directions while pre splitting rocks.

(3) Finally, through an analysis of the fracturing behavior exhibited by the overlying rock both prior to and subsequent to the implementation of the roof cutting procedure using EGB, the long cantilever structure was effectively shattered. This resulted in the filling of the goaf with gangue, thereby alleviating the pressure exerted on the roadway. The intricate mechanism underlying this relief of roof cutting pressure was meticulously unveiled, which subsequently facilitated the meticulous design of the parameters governing EGB. The outcomes derived from on-site experimental trials conclusively demonstrated that the synergistic implementation of EGB in conjunction with non-EGB successfully mitigated the stress and deformation of the two sides of the roadway in front of the mining face. The positive application effect observed in this study serves to furnish a comprehensive point of reference for addressing analogous engineering predicaments.

Author Contribution XX contributed significantly to the analysis and manuscript preparation; YZ contributed to the conception of the study; MH helped perform the analysis with constructive discussions; YG and YW contributed to the conception of the study; CZ and QF performed the data analyses and wrote the manuscript. All authors reviewed the manuscript.

Funding This work is supported by the National Key R&D Program of China (2022YFE0129100), and the China Postdoctoral Science Foundation (2022M723396), and the Fundamental Research Funds for the Central Universities (TU230003), and the Jiangsu Province Excellent Postdoctoral Program (2023ZB672), and Young Elite Scientists Sponsorship Program by Jiangsu (JSTJ-2023-JS015), which are gratefully acknowledged.

Data Availability The manuscript data used to support the findings of this study are available from the corresponding author upon request.

Declarations

Conflict of interest The authors have no relevant financial or non-financial interests to disclose.

Ethical Approval Not applicable.

Consent to Publish All authors agree to publish.

References

- Favreau RF (1969) Generation of strain waves in rock by an explosion in a spherical cavity. *J Geophys Res* 74(17):4267–4280
- Grady DE, Kipp ML (1987) Continuum modeling of explosive fracture in oil shale. *Int J Rock Mech Min* 17:147–157
- Guoli S, Chenglong X, Changda Z et al (2020) Fractal study on blasting damage of uncoupled charge with slotted charge. *China Min Ind* 29(03):105–109
- Harries G, Hengst B (1977) The use of a computer to describe blasting. *15th APCOM Symposiu* 24(3):317–324
- Huaibao C, Jinxing W, Xiaolin Y et al (2014) Study on the action mechanism of gas in the process of coal blasting damage and fracture. *J Min Saf Eng* 31(3):494–498
- Jiang F, Zhang S, Liu Y et al (2020) Damage evolution and radon exhalation rate response characteristics of radioactive rock under blasting dynamic load. *Chin J Rock Mech Eng* 39(S1):2741–2750
- Kang H, Wu L, Gao F et al (2019) Field study on the load transfer mechanics associated with longwall coal retreat mining. *Int J Rock Mech Min* 124:1
- Kingdom HY, Bo LW, Ming C et al (2012) Comparison and improvement of rock blasting damage model. *Rock Soil Mech* 33(11):3278–3284
- Kuzmaul JS (1987) New constitution model for fragmentation of rock under dynamic loading. *Oil Shales Tar Sands* 412–423

- Liang SR, Wei SL, Yao B et al (2014) Model test study on damage evaluation of frozen rock wall under blasting action. *Chin J Rock Mech Eng* 33(10):1945–1952
- Manchao He, Pengfei G, Xiaohu Z et al (2018) Directional presplitting of roadway roof based on two-way shaped charge tension blasting theory. *Exp Shock Waves* 38(04):795–803
- Taylor LM, Chen EP, Kusmaul J.s. (1986) Microcrack_Induced accumulation in brittle rock under dynamic loading. *Comput Method Appl Mech Eng* 55:301–320
- Throne BJ (1990) Experimental and computational investigation of the fundamental mechanics of cratering. *Inorg Org Phys Anal Chem* 117–124
- Xiaoding Xu, Yuejin Z, Shun P (2018) Analysis of catastrophic instability of plastic supporting system in old goaf of gypsum mine. *Chin J Rock Mech Eng* 37(11):2548–2555
- Xiaoding Xu, Yuejin Z, Yubing G et al (2023) Asymmetric floor heave mechanism and pressure relief control in composite bottom-slab roadways based on the three-hinged arch-spring model. *Chin J Rock Mech Eng* 42(06):1421–1433
- Xu X (2019) Study on stress blocking mechanism and evolution law of rock blasting roof cutting mining. China University of mining and technology
- Xu X, He M, Zhu C et al (2019) A new calculation model of blasting damage degree—based on fractal and tie rod damage theory. *Eng Fract Mech* 220:106619
- Xu M, Jiang J, Jiang T et al (2020) Hoek Brown elastoplastic damage model considering cyclic blasting effect and its engineering application. *Chin J Rock Mech Eng* 39:2683–2692
- Yang X (2000) Meso mechanism and mechanical properties of rock blasting damage and fracture. *Chin J Rock Mech Eng* 05:665
- Yang J, Jin Q (2018) Rock blasting damage model based on stress wave attenuation. *Explos Shock Waves* 2000:241–246
- Yang J, Lu W, Hu Y et al (2014) Cumulative damage characteristics of surrounding rock under repeated explosion load in tunnel excavation. *Rock and Soil Mechanics* 35(02):511–518
- Yang R, Xiao C, Li Y et al (2020) Fractal study on blasting damage of uncoupled eccentric charge structure. *J Vib Shock* 39(12):129–134
- Yang J, Qiang Fu, Gao Y et al (2023) A novel method of combined deep hole blasting for gob-side roadway protection. *Rock Mech Rock Eng* 56:3551–3571
- Yubing G, Jun Y, Xingyu Z et al (2019) Study on surrounding rock control technology of directional tension blasting for roof cutting and pressure relief in deep mine high stress roadway. *J Rock Mech Eng* 38(10):2045–2056
- Zou D (1985) Fragmentation distribution law of ore rock blasting and its application in blasting engineering. *Blasting* 02:35–41

Publisher's Note Springer Nature remains neutral with regard to jurisdictional claims in published maps and institutional affiliations.

Springer Nature or its licensor (e.g. a society or other partner) holds exclusive rights to this article under a publishing agreement with the author(s) or other rightsholder(s); author self-archiving of the accepted manuscript version of this article is solely governed by the terms of such publishing agreement and applicable law.